RESEARCH ARTICLE
ATMOSPHERIC PHYSICS

Earth and Planetary Physics
9: 1073–1086, 2025
doi: 10.26464/epp2025083

The stratospheric Brewer–Dobson circulation under different phases of the Stratospheric Polar Vortex Oscillation combined with different phases of the Quasi-Biennial Oscillation

ZiXuan Yu, ChunHua Shi*, Jian Rao, and YueYue Yu

State Key Laboratory of Environment Characteristics and Effects for Near-space/School of Atmospheric Sciences, Nanjing University of Information Science and Technology, Nanjing 210044, China

Key Points:

- The strength of Brewer–Dobson circulation (BDC) anomalies driven by gravity waves in the upper stratosphere reaches approximately half that of the anomalies driven by planetary waves.
- The Quasi-Biennial Oscillation (QBO) controls the vertical position of the anomaly center within the BDC's descending branch.
- Under strong boreal stratospheric polar vortex (BSPV) conditions, the influence of the QBO on the austral subpolar stratospheric BDC is more pronounced than that under weak BSPV conditions.

Citation: Yu, Z. X., Shi, C. H., Rao, J., and Yu, Y. Y. (2025). The stratospheric Brewer–Dobson circulation under different phases of the Stratospheric Polar Vortex Oscillation combined with different phases of the Quasi-Biennial Oscillation. *Earth Planet. Phys.*, *9*(5), 1073–1086. http://doi.org/10.26464/epp2025083

Abstract: Using long-term Whole Atmosphere Community Climate Model version 5 (WACCM5) simulations initialized with the climatology around the year 2000, we studied the anomalous distribution of planetary wave and gravity wave fluxes during distinct phases of the boreal stratospheric polar vortex (BSPV) and Quasi-Biennial Oscillation (QBO). The contributions of these two types of waves to Brewer–Dobson circulation (BDC) anomalies were further analyzed. The results revealed that under four distinct phases, the northern hemisphere BDC is primarily governed by planetary waves, whereas gravity waves counteract approximately half of the planetary wave influence on the BDC in the upper stratosphere. The QBO regulates the position of the anomaly center within the BDC's descending branch in the northern hemisphere. In particular, during the westerly phase of the QBO (WQBO), the center of this anomalous descending branch is located in the upper stratosphere, whereas during the easterly phase of the QBO (EQBO), it is located in the lower stratosphere. Southern hemisphere BDC anomalies are regulated more by QBO activity: during the WQBO, it shows synchronous changes with the BDC anomaly in the northern hemisphere, whereas during the EQBO, it exhibits an antiphase relationship with the BDC anomaly in the northern hemisphere. Mesospheric circulation anomalies are predominantly driven by gravity wave activity. The circulation weakens during a weak BSPV and strengthens during a strong BSPV. Additionally, the descending branch anomaly of the northern hemisphere circulation is more pronounced during the WQBO, whereas the ascending branch anomaly of the southern hemisphere circulation is more significant during the EQBO.

Keywords: Brewer–Dobson circulation; quasi-biennial oscillation; stratospheric polar vortex; planetary wave; gravity wave

1. Introduction

The middle-atmosphere Lagrangian meridional circulation, also known as the Brewer–Dobson circulation (BDC), is an important component of the Earth's climate that plays a very important role in troposphere–stratosphere material exchange and the global material–energy balance. The breaking of gravity waves is the primary driver of the mesospheric summer to winter pole meridional circulation, whereas Rossby waves (including planetary waves and synoptic-scale waves) are the key factors driving the stratospheric circulation. The stratospheric BDC can be further divided into deep and shallow branches (Birner and Bönisch, 2011; Butchart, 2014). The deep branch, located in the middle to upper stratosphere of the winter hemisphere, is predominantly driven by planetary waves, whereas the two shallow branches reside in the lower stratosphere of both hemispheres and are primarily forced by synoptic-scale waves.

Research suggests that radiative effects, planetary waves, and the evolution of the zonal mean wind all contribute differently to the strength of the BDC. Some studies have utilized indirect methods to characterize the effects of gravity waves and have demonstrated that they not only influence the low-latitude portion of the shallow branch of the BDC during winter but also drive the poleward extension of the deep branch of the BDC in seasons other than

First author: Z. X. Yu, 3295893498@qq.com
Correspondence to: C. H. Shi, shi@nuist.edu.cn
Received 25 APR 2025; Accepted 27 JUN 2025.
First Published online 29 JUL 2025.

summer (Sato and Hirano, 2019). Other studies (Butchart and Scaife, 2001; Butchart et al., 2006, 2010) have confirmed that the strengthening of the BDC is related to increased stratospheric drag caused by resolved waves (planetary waves) and small-scale gravity waves. In addition, background flow, such as the strengthening of the subtropical upper tropospheric jet stream, increases the breaking height of orographic gravity waves, allowing more gravity wave momentum flux to enter the stratosphere, thereby increasing the orographic gravity wave drag in the lower stratosphere (Li F et al., 2008; McLandress and Shepherd, 2009).

Changes in wave activity in the stratosphere typically originate from two sources: the troposphere and internal changes in the stratosphere. The former depends on convective activity, topography, sea surface temperature and ice, snow cover, blocking, and other underlying surface forcing, as well as planetary waves and gravity waves propagating upward caused by dynamic processes within the troposphere. The latter mainly involves the stratosphere's own regulation of the wave generation–propagation environment. The Quasi-Biennial Oscillation (QBO) and the stratospheric polar vortex, as significant dynamic processes within the stratosphere, have a nonnegligible impact on the propagation of planetary waves and gravity waves.

The boreal stratospheric polar vortex (BSPV) is a core component of the large-scale circulation system in the winter stratosphere and plays a significant role in the coupling process between the stratosphere and troposphere (Li Q et al., 2011; Zhang JK et al., 2023; Xie F et al., 2024; Zhang CY et al., 2024). Variations in the northern hemisphere BSPV are driven primarily by slow radiative cooling and rapid dynamic disturbances. The dynamic disturbances mainly originate from planetary-scale Rossby waves propagating upward from the troposphere (Butchart, 2022; Tian WS et al., 2023). Additionally, when anomalies exist in the BSPV because of changes in stratospheric winds, the BSPV's filtering of gravity waves also changes, thereby affecting mesospheric circulation (Azeem et al., 2005; de Wit et al., 2015). Large-scale circulation changes related to BSPV anomalies can also lead to the generation of new waves (Tomikawa et al., 2012; Chandran et al., 2013; Yu FR et al., 2019). Changes in the strength of the BSPV can not only alter the dynamic and thermal structure of the stratospheric BDC but can also have a profound effect on surface weather and climate through stratosphere–troposphere coupling mechanisms (Baldwin and Dunkerton, 2001; Limpasuvan et al., 2004; Martineau and Son, 2010; Rao J and Garfinkel, 2020).

A strong link also exists between the stratospheric QBO and the BSPV in the northern hemisphere, a relationship often referred to as the Holton–Tan relationship (Holton and Tan, 1980, 1982; Garfinkel et al., 2012; Anstey and Shepherd, 2014; Xie F et al., 2020). Specifically, under the easterly phase of the QBO (EQBO) in the lower stratosphere, more of the active stratospheric planetary wave flux propagates poleward and the polar vortex is weaker during northern hemisphere winters, whereas under the westerly phase of the QBO (WQBO), the opposite is true. The QBO can be seen to influence the BDC by modulating atmospheric fluctuations on the one hand and the BSPV on the other hand, which is further correlated with tropospheric circulation anomalies such as the Arctic Oscillation (Rao J et al., 2019; Zhang RH et al., 2020; Cai QY et al., 2022).

Both the BSPV and the QBO exhibit strong connections with the BDC, with their underlying mechanisms involving wave-related processes. Current studies investigating planetary and gravity wave impacts on the BDC predominantly utilize filtering techniques to extract or suppress gravity waves. However, such fixed-wavenumber filtering approaches introduce errors because of the altitude-dependent wavelength variations of gravity waves. Furthermore, constrained by vertical resolution limitations in reanalysis data, many studies inadequately account for mesospheric gravity wave contributions. Although gravity waves primarily exert their influence in the mesosphere, the "downward control" principle dictates that upper-level anomalies can dynamically couple with lower atmospheric layers. This mechanism implies that mesospheric gravity wave anomalies can modulate stratospheric BDC variability—an influence that cannot be neglected in comprehensive dynamic analyses.

In the present study, we utilize gravity wave data directly outputted from Whole Atmosphere Community Climate Model version 5 (WACCM5) model simulations and extracted planetary wave data to analyze the impacts of planetary and gravity waves on the stratospheric BDC under varying combinations of QBO phases and polar vortex anomalies. We also investigate potential dynamic mechanisms.

2. Data and Methods

2.1 Data

In this study, we use the atmospheric chemistry climate model WACCM5. The atmospheric part of the WACCM5 uses the physical parameterization scheme of the Community Atmosphere Model version 5 (CAM5), which can closely simulate the dynamics, radiation, and chemical processes of the stratosphere–troposphere. Furthermore, in this study we use a version of the WACCM in which QBO forcing is prescribed at a periodicity of approximately 28 months, which successfully reproduces the modulation effects of QBO variability on atmospheric circulation patterns. In addition, the WACCM5 includes simulations of the chemical composition, and the simulation domain covers the lower thermosphere from the ground up to approximately 4.5×10^{-6} hPa, which includes the mesosphere dominated by gravity waves. It can therefore better describe the effect of gravity waves on the BDC. The horizontal resolution of the numerical simulation in this study is $2° \times 2°$, with 70 layers in the vertical direction. The initial value used is Fw2000 (the climatology from 1995 to 2005) and is conducted over 40 model years, with the first 5 years allocated as the spin-up period. The output results include daily meridional wind, zonal wind, vertical velocity, temperature, geopotential height, and gravity wave flux, among others.

2.2 Methods

2.2.1 Representation of the BDC

The transformed Eulerian mean zonal momentum equation and thermodynamic energy equation of the middle atmosphere are as follows:

$$\frac{\partial [u]}{\partial t} - \hat{f}[v]^* + [w]^* \frac{\partial [u]}{\partial z} = \frac{1}{\rho_0 a \cos\phi} \nabla \boldsymbol{F} + [\mathrm{GWF}] + [X], \tag{1}$$

$$\frac{\partial [\theta]}{\partial t} + \frac{[v]^*}{a} \frac{\partial [\theta]}{\partial \phi} + [w]^* \frac{\partial [\theta]}{\partial z} = [Q] - \frac{1}{\rho_0} \frac{\partial}{\partial z} \left[\rho_0 \left(\frac{[\theta' v']}{a \theta_z} + [w' v'] \right) \right], \tag{2}$$

where the prime symbols (′) denote deviations from the zonal mean, w is the vertical velocity, a is the radius of the Earth, u is the zonal wind, $[v]^*$ is the meridional residual velocity, $[w]^*$ is the vertical residual velocity, ϕ is the latitude, ρ_0 is the atmospheric density, $\hat{f} = f - \frac{1}{a\cos\phi} \frac{\partial ([u]\cos\phi)}{\partial \phi}$, where f is the geostrophic parameter, $\nabla \boldsymbol{F}$ is the Eliassen-Palm (E-P) flux divergence caused by planetary waves, GWF is the resistance caused by gravity waves, X represents frictional and viscous resistance, and brackets indicate the zonal average. The calculations of $[v]^*$, $[w]^*$, $\nabla \boldsymbol{F}$, and GWF are as follows:

$$\begin{cases} F(\phi) = -\rho_0 a \cos\phi [u'v'], \\ F(z) = \rho_0 f a \cos\phi \dfrac{[\theta' v']}{[\theta]_z}, \end{cases} \tag{3}$$

$$\nabla \boldsymbol{F} = \frac{1}{a\cos\phi} \frac{\partial}{\partial \phi} (F(\phi)\cos\phi) + \frac{\partial}{\partial z} (F(z)), \tag{4}$$

$$[\mathrm{GWF}] = \frac{1}{\rho_0} \frac{\partial \left(-\rho_0 \left(1 - \dfrac{f^2}{\omega^2} \right) [u'w'] \right)}{\partial z}, \tag{5}$$

$$\begin{cases} [v]^* = [v] - \dfrac{1}{\rho} \left(\dfrac{\rho [v'\theta']}{[\theta]_z} \right)_z, \\ [w]^* = [w] - \dfrac{1}{a\cos\phi} \left(\dfrac{\cos\phi [v'\theta']}{[\theta]_z} \right)_\phi, \end{cases} \tag{6}$$

where ω in Equation (5) is the gravity wave frequency. The momentum in Equation (1) shows that the residual velocity ($[v]^*$,$[w]^*$) is related to the variation of the mean westerly momentum (u) and the fluctuating driving term. To characterize the mean meridional circulation, a meridional mass stream function (ψ^*) is defined:

$$\psi^* = \int_z^\infty [v]^* \rho \cos\phi \mathrm{d}z, \tag{7}$$

and ($[v]^*$,$[w]^*$) can be represented as

$$\begin{cases} [v]^* = -\dfrac{1}{\rho \cos\phi} \cdot \dfrac{\partial \psi^*}{\partial z}, \\ [w]^* = \dfrac{1}{a\rho\cos\phi} \cdot \dfrac{\partial \psi^*}{\partial \phi}. \end{cases} \tag{8}$$

Considering the case in which the monthly scale is close to constant and the vertical motion term is neglected, the $[v]^*$ in Equation (1) is related to the gravity wave, the planetary wave, and the residual term, respectively. Therefore, the corresponding mass stream function can be expressed as

$$\psi^*(\phi, z) = \psi_{\mathrm{PW}}(\phi, z) + \psi_{\mathrm{GW}}(\phi, z) + \psi_X(\phi, z), \tag{9}$$

where

$$\psi_{\mathrm{PW}} = -\int_z^\infty \frac{\nabla \boldsymbol{F}}{a\hat{f}} \mathrm{d}z, \tag{10}$$

$$\psi_{\mathrm{GW}} = -\cos\phi \int_z^\infty \frac{\rho}{\hat{f}} [\mathrm{GWF}] \mathrm{d}z, \tag{11}$$

$$\psi_X = -\cos\phi \int_z^\infty \frac{\rho}{\hat{f}} [X] \mathrm{d}z. \tag{12}$$

Because the object of this study is the stratosphere and mesosphere, the friction and viscous terms are neglected here, that is, in Equation (12). Therefore, Equations (10) and (11) can be used to study the contribution of the upper planetary and gravity waves to the lower BDC, which is known as the downward control (Andrews and McIntyre, 1976; Haynes et al., 1991; Rosenlof and Holton, 1993).

2.2.2 Definition of a strong and weak BSPV and QBO

In this study, with reference to the two BSPV intensity indices, the northern hemisphere winter months (from November to February, NDJF), in which both are less than −0.5 times the standard deviation, are treated as weak BSPV months, whereas the months in which they are greater than 0.5 times the standard deviation are treated as strong BSPV months. The first BSPV index characterizes the strength of the polar vortex by the geopotential height anomaly of the weighted average of the 10 hPa polar regions (Kolstad et al., 2010):

$$Z_P = -\sum (Z' \cos\phi) \Big/ \sum \cos\phi, \tag{13}$$

where Z_P is the BSPV index, Z' is the anomaly in the zonal mean geopotential height relative to the climatology, and $\sum$ is the sum over the area north of 65°N. The Z_P was standardized for use in this study. The second BSPV index is derived from the standardized time series of zonal mean zonal wind anomalies at 10 hPa over 60°N–70°N.

The QBO index is defined as the zonal mean zonal wind anomalies standardized at 10 hPa between 5°S and 5°N. When the standardized anomalies exceed +0.5 standard deviations, they are classified as the WQBO; when they are below −0.5 standard deviations, they are classified as the EQBO.

2.2.3 Composite analysis

From the WACCM5 simulation results, four different combinations of tropical stratospheric WQBO or EQBO with strong or weak BSPV in the northern hemisphere winter are selected for classification. The corresponding winter months that satisfy the classification are selected to analyze the planetary wave and gravity wave active flux divergence and BDC stream function anomalies in each classification month so as to obtain the effect of different combinations of QBO and BSPV perturbations on the BDC and the contribution of different waves.

3. Results

3.1 Performance Assessment of Northern Hemisphere Winter Circulation Simulations

First, we evaluate whether the mass stream function derived from planetary and gravity wave dissipation through the downward control principle can accurately represent the BDC in the northern

hemisphere winter atmosphere. Because the downward control principle is inapplicable for calculating the mass stream function in low latitudes, Figure 1 compares only extratropical differences between the mass stream function obtained via this principle and that derived from residual velocity integration. In Figure 1a, the stream function (shaded) driven by planetary and gravity waves, as well as the total stream function (contours), exhibits a relatively consistent circulation structure in the mid to high latitudes (50°–80°) of both hemispheres in the stratosphere and mesosphere. This structure effectively reflects the closed hemispheric BDC in the southern and northern stratospheres, as well as the global BDC in the mesosphere, which is characterized by ascent at the South Pole and descent at the North Pole. At the isobaric surfaces representing the stratosphere, mesosphere, and transition layer, respectively (Figures 1b–1f), the mass stream function lines calculated by the two methods between 50° and 80° in the northern and southern hemispheres are relatively close, and their meridional gradients (representing vertical velocity) are also relatively close. This result indicates that, at this location, the portion driven by planetary and gravity waves can approximately explain the entire BDC. At other latitudes, a large difference exists in the stream functions calculated by the two methods, and it is possible that the effect of diabatic heating on the residual velocities cannot be ignored in these regions (Equation (2)). Therefore, our discussion of the BDC in the following text is limited to high-latitude regions in the northern and southern hemispheres.

During a weak BSPV (Figures 2a and 2b), in the mid to high latitudes of the northern hemisphere, the weak easterly winds in the upper

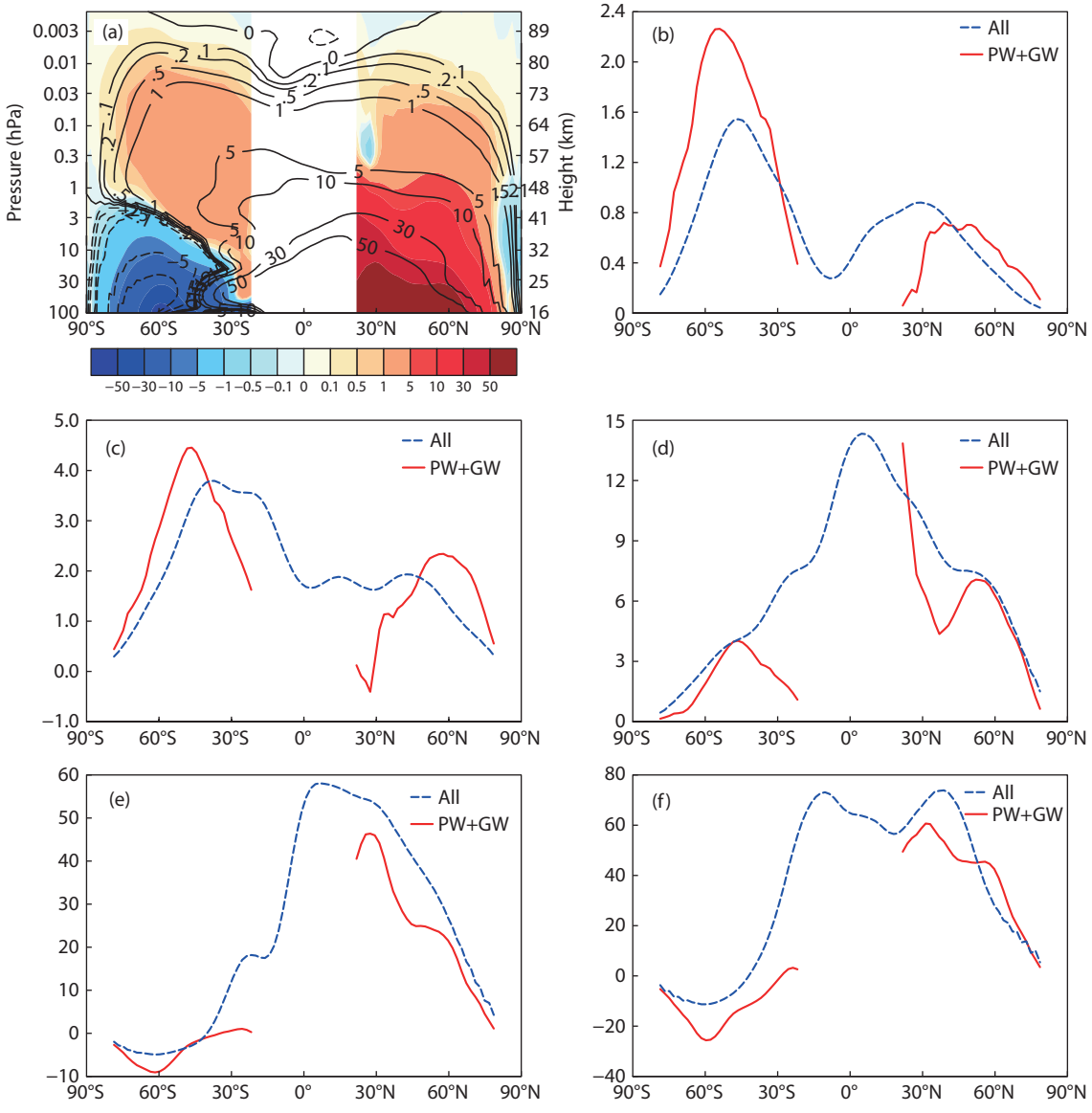

Figure 1. Multiple-year averaged NDJF mass stream function (unit: kg·s^{-1}m^{-1}): (a) BDC mass stream function driven by the dissipation of planetary and gravity waves (derived from Equations (10) and (11), shaded), and mass stream function obtained by integrating the residual velocity (v^*, derived from Equations (6) and (7), contours); (b–f) the mass stream function driven by the dissipation of planetary and gravity waves (solid red curves) and the mass stream function obtained by integrating the residual velocity (dashed blue curves) at the isobaric surfaces of 0.03, 0.1, 1, 10, and 30 hPa. PW, planetary wave; GW, gravity waves.

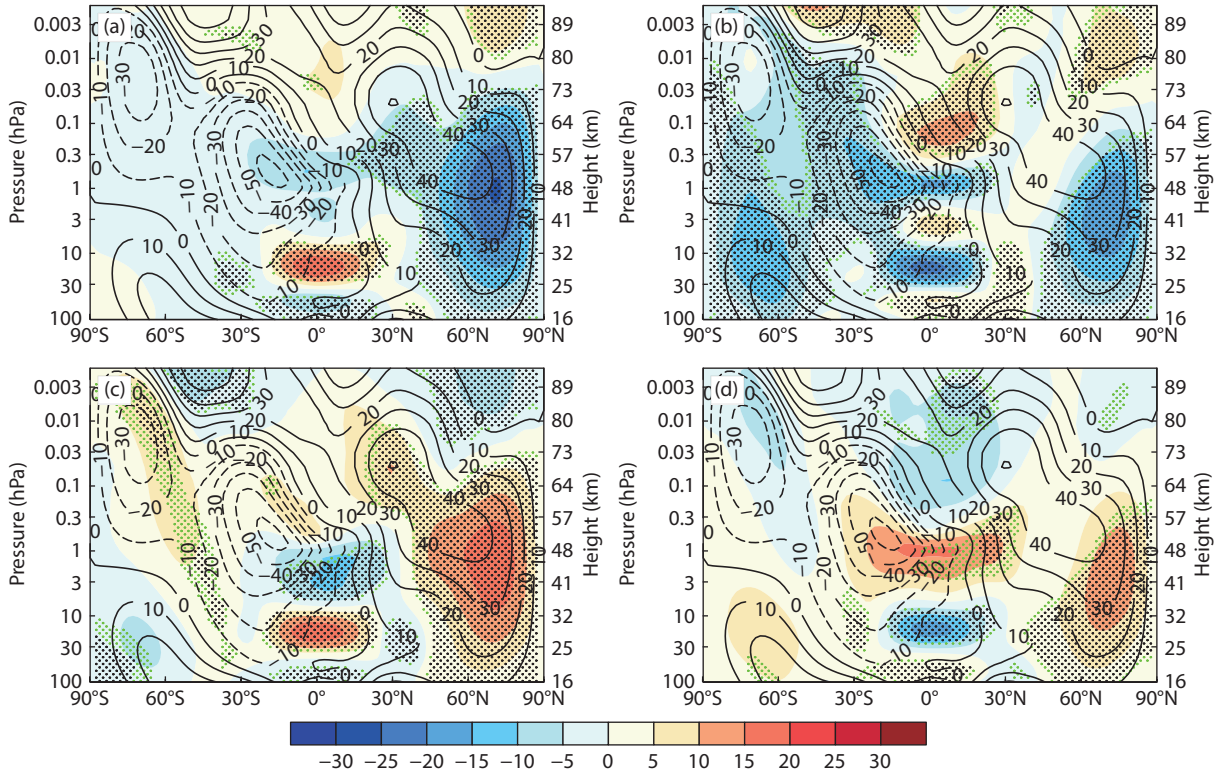

Figure 2. The zonal mean zonal wind anomalies of four combined phases of the BSPV disturbance and QBO in NDJF (shaded; unit: m·s^{-1}) and its climatology (contours; unit: m·s^{-1}). Areas that exceed the 95% (90%) significance level are marked with black (green) dots. (a) Under the conditions of a weak BSPV and the WQBO; (b) under the conditions of a weak BSPV and the EQBO; (c) under the conditions of a strong BSPV and the WQBO; (d) under the conditions of a strong BSPV and the EQBO.

middle mesosphere weaken, and the westerly winds in the stratosphere weaken significantly, especially during the WQBO, where the maximum wind anomaly in the upper stratosphere reaches −30 m·s^{-1} (Figure 2a). During the EQBO, the negative anomaly of the westerly winds in the northern hemisphere stratosphere decreases to no more than 20 m·s^{-1}, whereas in the lower stratosphere of high latitudes in the southern hemisphere, an easterly wind anomaly occurs, causing the summer stratospheric east wind belt of the southern hemisphere to abnormally extend toward the polar lower stratosphere (Figure 2b).

During the strong BSPV, the zonal wind anomaly characteristics are almost the opposite those during the weak BSPV. During this period, the intensity and coverage of the westerly wind anomaly in the mid- to high-latitude stratosphere of the northern hemisphere are more pronounced during the WQBO. However, compared with the weak BSPV period, the zonal wind anomalies in the southern hemisphere stratosphere during the EQBO are not significant.

The downward control principle indicates that the strength of the BDC is directly related to planetary waves, gravity waves, and other oscillations. In model data, planetary waves modulate the atmospheric circulation by transporting zonal wind eddy momentum in the meridional direction. The average unit volume of planetary wave flux divergence in the extratropical stratosphere is negative, meaning that the westward eddy momentum flux converges here, with a more pronounced effect in the northern hemisphere (Figure 3a). As shown in Equation (1), this convergence of westward momentum flux not only slows down the background westerly jet, but also, through the geostrophic effect, drives the formation of a poleward BDC in both hemispheres. The stronger wave flux convergence in the northern hemisphere corresponds to a stronger BDC, which aligns well with previous studies (Diallo et al., 2021). This finding suggests that the numerical model successfully simulates the climatology of a planetary wave-driven BDC.

Gravity waves modulate large-scale circulation by vertically transporting momentum flux. In the stratosphere, gravity waves exhibit momentum flux convergence, similar to planetary waves but with a weaker intensity. However, in the southern hemisphere mesosphere, gravity waves exhibit momentum flux divergence, inducing the air eastward acceleration. And in the northern hemisphere mesosphere, gravity waves exhibit momentum flux convergence, producing westward acceleration (Figure 3b). That is, gravity waves act to weaken the westerly winds in the northern hemisphere mesosphere and the easterly winds in the southern hemisphere mesosphere. The spatial distribution of this momentum flux divergence, on one hand, drives the climatology of mesospheric circulation through the geostrophic effect with the air ascent in the high latitudes of the southern hemisphere and descent in the high latitudes of the northern hemisphere; on the other hand, it influences the stratospheric BDC through the downward control principle. Previous studies of stratospheric BDC anomalies have often emphasized the driving source anomalies of stratospheric planetary waves (Figure 3a) while anomalies driven

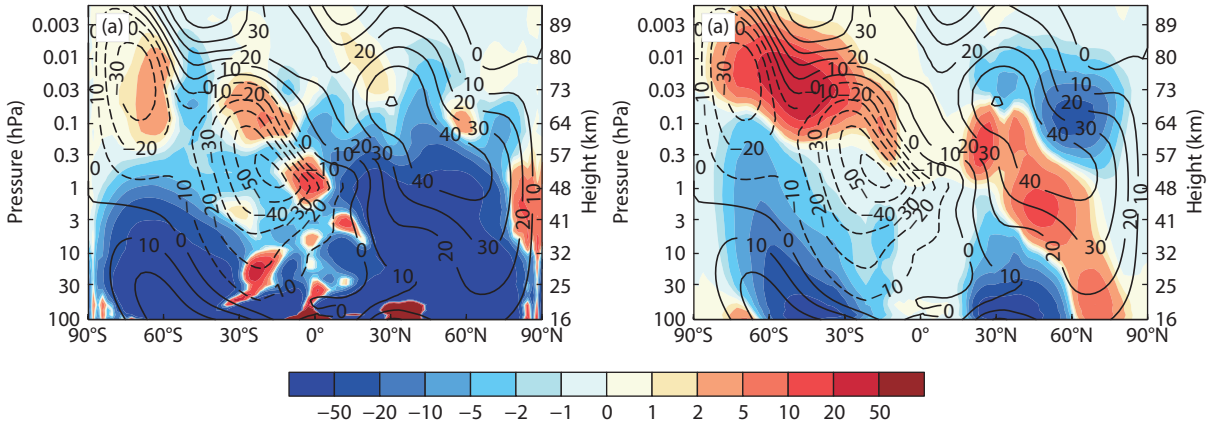

Figure 3. NDJF-averaged zonal wind (contours; unit: m·s^{-1}) and (a) planetary wave E-P flux divergence ($\frac{1}{a\cos\phi}\nabla \boldsymbol{F}$, shaded; unit: 10^{-9} kg·s^{-2}m^{-2}); (b) vertical gradient of the eddy momentum flux of gravity waves (ρ_0 [GWF], shaded; unit: 10^{-9} kg·s^{-2}m^{-2}).

by mesospheric gravity waves (Figure 3b) have been neglected (Sato and Hirano, 2019; Diallo et al., 2021).

3.2 Forcing Anomalies of Planetary and Gravity Waves on the BDC in Different Combinations of the BSPV and QBO

During a weak BSPV and the WQBO, a planetary wave active flux convergence anomaly occurs in the extratropical upper and middle stratosphere of the northern hemisphere, which strengthens the climatology of wave active flux convergence at that location. A similar situation also appears in the middle stratosphere of the southern hemisphere extratropics (Figure 4a). During a weak BSPV and the EQBO period, the planetary wave active flux divergence anomalies cover almost the entire extratropical stratosphere of the southern hemisphere, weakening the climatology of wave active flux convergence at that location (Figure 4b). In the extratropical stratosphere of the northern hemisphere, the wave flux convergence anomalies are stronger in intensity and their positions are more biased toward the lower stratosphere compared with the WQBO period, thereby enhancing the deceleration effect of the wave motion on the background westerly winds (Figure 4b). During a strong BSPV, the wave active flux in the stratosphere of

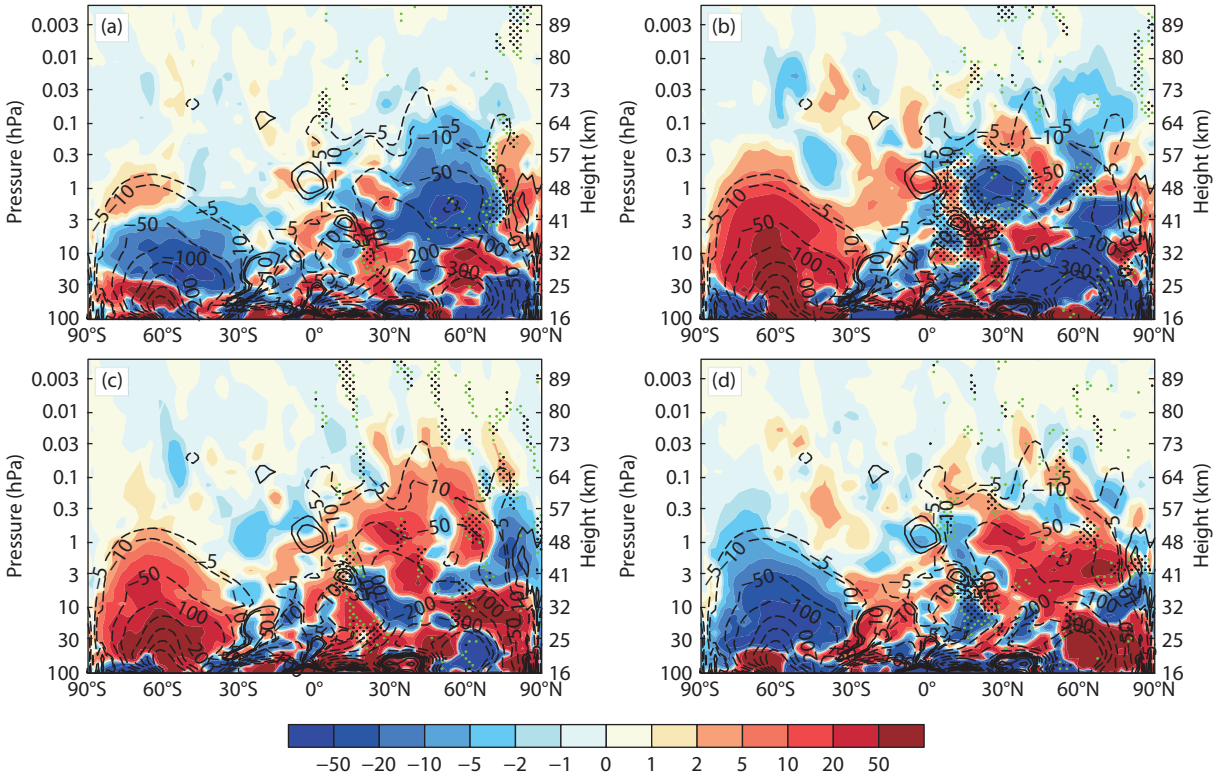

Figure 4. As in Figure 2, but with the climatology of planetary wave E-P flux divergence (contours; unit: 10^{-9} kg·s^{-2}m^{-2}) and its anomaly (shaded; unit: 10^{-9} kg·s^{-2}m^{-2}). (a) Under the conditions of a weak BSPV and the WQBO; (b) under the conditions of a weak BSPV and the EQBO; (c) under the conditions of a strong BSPV and the WQBO; (d) under the conditions of a strong BSPV and the EQBO.

the southern hemisphere exhibits divergence anomalies during the WQBO, weakening the climatology of wave active flux convergence at that location (Figure 4c); the opposite occurs during the EQBO period (Figure 4d). However, in the extratropical stratosphere of the northern hemisphere, both the WQBO and EQBO periods are characterized by planetary wave active flux divergence anomalies (Figures 4c and 4d). In general, planetary wave anomalies in the northern hemisphere exhibit stronger correlations with the BSPV, with enhanced dissipation of background planetary waves during a weak BSPV and the opposite during a strong BSPV. In the southern hemisphere, planetary wave anomalies are closely linked to both the QBO and the BSPV. During the WQBO period, the wave anomalies in the southern hemisphere are consistent with those in the northern hemisphere. However, during the EQBO period, the wave anomalies in the southern hemisphere are opposite those in the northern hemisphere.

Because of the background gravity wave dissipation having two centers in the stratosphere and mesosphere (Figure 3b) during different phases of the BSPV and QBO disturbances, the abnormal centers with a larger momentum flux often appear in these two locations. During the weak BSPV, a significant divergence anomaly of gravity wave momentum flux exists in the northern hemisphere mesosphere, which weakens the climatological gravity wave effect at this location. In contrast, in the middle to lower stratosphere of the northern hemisphere mid to high latitudes, there is a convergence anomaly of gravity wave momentum flux. The anomaly intensities of gravity wave momentum flux divergence in the northern hemisphere mesosphere and stratosphere are larger during the WQBO period (Figures 5a and 5b). The gravity wave momentum flux divergence anomaly in the southern hemisphere is stronger during the EQBO period, with divergence anomalies of gravity wave momentum flux in the extratropical upper and middle stratosphere (Figure 5b). During a strong BSPV, the abnormal effects of gravity waves in the northern hemisphere occur at positions similar to those during a weak BSPV, but with opposite effects (Figures 5c and 5d). Theoretically, the propagation of gravity waves is filtered by the background zonal wind vertical gradient. In the strong and weak BSPV, the maximum anomaly center of the circumpolar westerly winds in the northern hemisphere is near (70°N, 1 hPa; Figure 2). Therefore, the anomaly centers of gravity wave momentum flux divergence in the northern hemisphere are located above and below this zonal wind anomaly center, with opposite signs.

3.3 Contributions of Planetary and Gravity Wave Anomalies to BDC Anomalies in Different Combinations of the BSPV and QBO

During NDJF, the stratospheric BDC is primarily driven by planetary waves, with poleward circulation along the positive contours of the mass stream function in the northern hemisphere (Figure 6a), and with poleward circulation along the negative contours in the southern hemisphere. Additionally, the absolute values of the meridional gradients of the mass stream function at high latitudes (indicating the descending velocity) are greater in the northern hemisphere than in the southern hemisphere. The BDC driven by gravity waves is mainly concentrated in the upper stratosphere

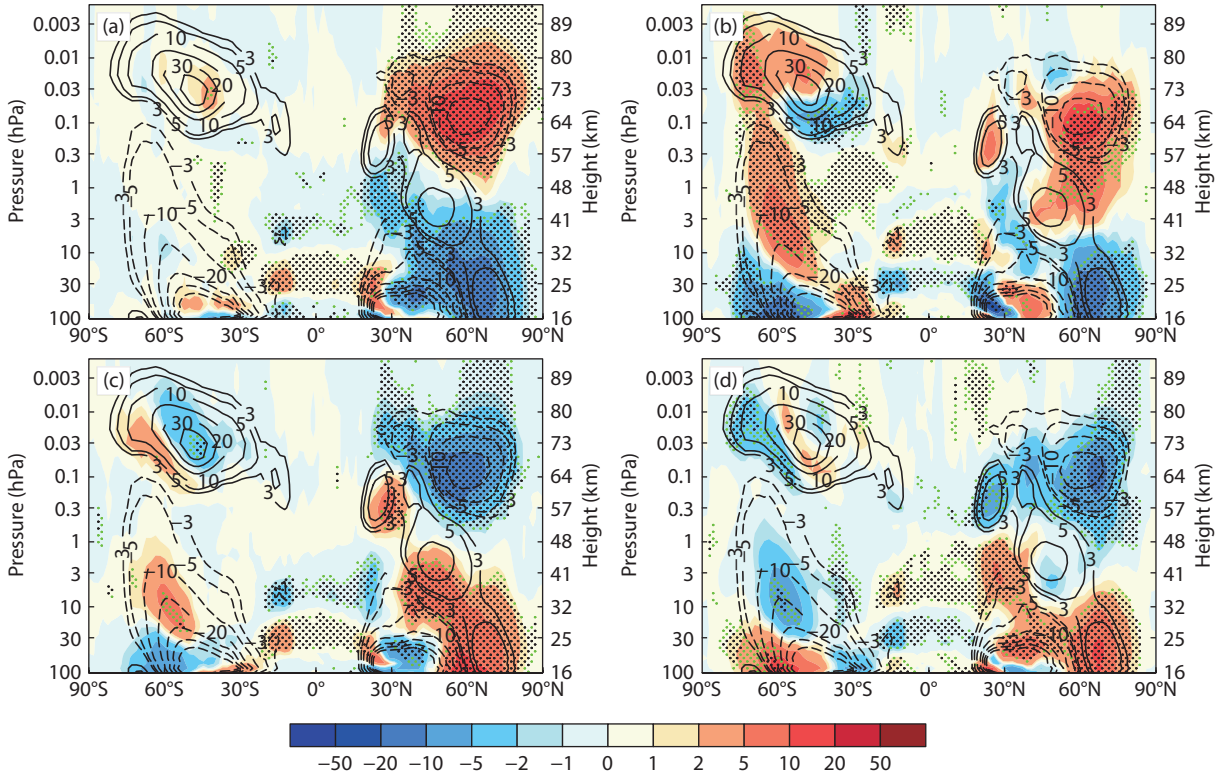

Figure 5. As in Figure 2, but for the climatology of the vertical gradient of momentum flux of the gravity wave (contours; unit: 10^{-9} kg·s^{-2}m^{-2}) and its anomaly (shaded; unit: 10^{-9} kg·s^{-2}m^{-2}). (a) Under the conditions of a weak BSPV and the WQBO; (b) under the conditions of a weak BSPV and the EQBO; (c) under the conditions of a strong BSPV and the WQBO; (d) under the conditions of a strong BSPV and the EQBO.

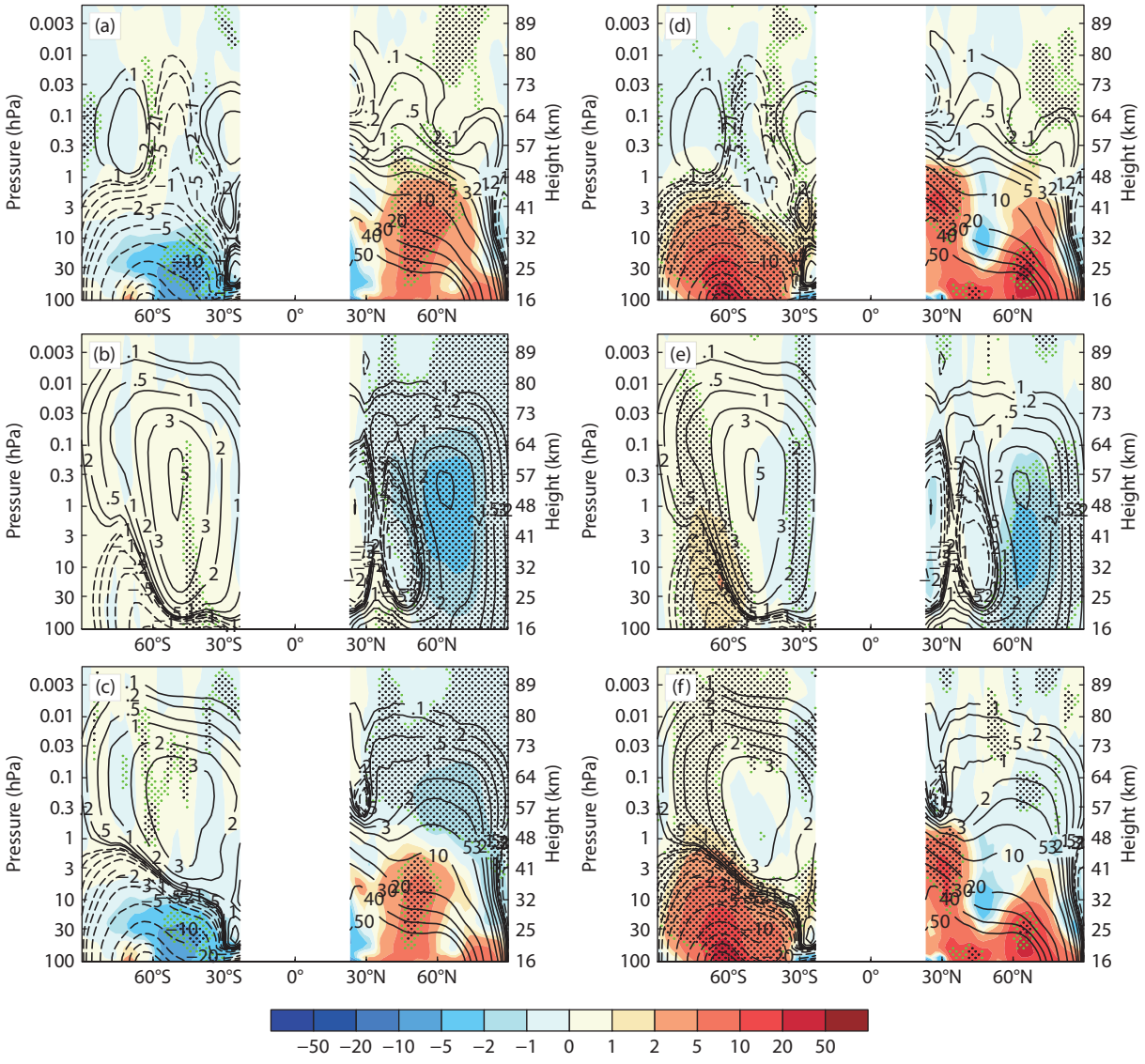

Figure 6. Climatology of the mass stream function in NDJF (contours; unit: kg·m^{-1}s^{-1}) and its anomaly (shaded; unit: kg·m^{-1}s^{-1}) under the background of a weak BSPV. (a) Mass stream function anomaly driven by planetary waves during the WQBO; (b) mass stream function anomaly driven by gravity waves during the WQBO; (c) mass stream function anomaly driven by both planetary and gravity waves during the WQBO; (d–f) as in (a) to (c), respectively, but during the EQBO.

and mesosphere of both hemispheres, with clockwise circulation along the positive contours of the mass stream function, where air ascends over Antarctica and descends over the Arctic (Figure 6b). When gravity waves and planetary waves act together, the mass circulation exhibits a composite feature: in the mesosphere, the mass stream function resembles the case driven solely by gravity waves, whereas in the stratosphere, the mass stream function is closer to the distribution under the planetary wave influence alone (Figure 6c).

Under weak polar vortex conditions, during both the WQBO and EQBO periods, the planetary wave anomaly-driven mass stream function in the northern hemisphere stratosphere exhibits positive anomalies, with anomaly centers coinciding with the center of climatology, thereby increasing the high-latitude meridional gradient, which strengthens the BDC descending branch in the northern hemisphere high latitudes (Figures 6a and 6d). Similarly, in the southern hemisphere, during the WQBO periods, the mass stream function shows negative anomalies, with increased high-latitude meridional gradients, strengthening the BDC, whereas during the EQBO periods, the mass stream function exhibits positive anomalies, with decreased high-latitude meridional gradients, weakening the BDC. At this time, the gravity wave-driven BDC weakens in the northern hemisphere stratosphere and mesosphere, with the BDC anomaly center position being lower and weaker during the EQBO compared with the WQBO (Figures 6b and 6e), whereas in the southern hemisphere mesosphere, the BDC intensity strengthens slightly.

The anomalies of the mass stream function driven jointly by planetary waves and gravity waves during a weak BSPV are dominated by planetary wave-driven anomalies in the stratosphere and gravity wave-driven anomalies in the mesosphere (Figures 6c and 6f). It is worth noting that in the northern hemisphere stratosphere,

because the stream function anomalies driven by gravity waves are opposite those driven by planetary waves, the mass stream function anomaly intensity decreases compared with anomalies driven solely by planetary waves, and the significant anomaly regions also shrink or even disappear. This finding is inconsistent with the phenomenon observed in Figures 4a–4b and 5a–5b, where the flux divergence anomalies of planetary waves and gravity waves in the northern hemisphere stratosphere are of the same sign. This result indicates that the gravity wave flux divergence anomalies in the mesosphere, which are opposite those in the stratosphere, as shown in Figures 4a–4b and 5a–5b, can still have a significant impact on the BDC anomalies in the stratosphere below.

The intensity of the BDC is typically represented by the residual velocity in the vertical direction (Sato and Hirano, 2019); thus, w^* can be further used to assess the effects of planetary waves and gravity waves on the BDC. The analysis in Figure 1 shows that the mass stream functions driven by planetary waves and gravity waves, along with the corresponding residual vertical velocity, are very close to the actual situation in the high latitudes of both the southern and northern hemispheres. Therefore, the following analysis focuses on the representative residual vertical velocity w^* in the high latitudes. During NDJF, the climatology of w^*, driven jointly by planetary waves and gravity waves, shows air ascending near 70°S (Figure 7a) and air descending near 70°N (Figure 7g) in the mesosphere, whereas in the stratosphere, air descends in the high latitudes of both hemispheres (Figures 8b, 8c, 8h, and 8i).

Under weak BSPV conditions, the w^* anomalies in the high-latitude mesosphere associated with different QBO phases exhibit patterns opposite the climatology in both hemispheres, indicating a weakened BDC. This effect is more pronounced in the northern hemisphere during the WQBO and in the southern hemisphere during the EQBO (Figures 7a and 7j). These w^* anomalies are primarily driven by gravity waves.

The w^* anomaly sinks at high latitudes in the northern hemisphere stratosphere during a weak BSPV, which represents the strengthening of the BDC, with this effect being more significant in the upper-middle stratosphere during the WQBO. Here, the w^* anomaly is dominated by planetary wave-driven anomalies, with gravity wave-driven anomalies acting opposite, cancelling out about half of the planetary wave effect (Figure 7b). In the middle-lower stratosphere, the BDC also strengthens, which is more pronounced during the EQBO, dominated by planetary wave-driven anomalies, whereas gravity wave-driven anomalies are relatively negligible (Figure 7f).

In the southern hemisphere, w^* anomalies in the high-latitude stratosphere rise during the EQBO, contrary to the climatology, leading to a weakened BDC. In the upper-middle stratosphere, planetary wave-driven and gravity wave-driven w^* anomalies are synchronized and of comparable magnitudes (Figure 7k). However, in the middle-lower stratosphere, the weakening of the BDC is primarily driven by planetary wave anomalies (Figure 7l).

Under strong BSPV conditions, the planetary wave-driven stream function anomalies (Figures 8a and 8d) are opposite those under weak BSPV conditions (Figures 6a and 6d). During both the WQBO and EQBO, the stream function anomalies in the northern hemisphere are negative, whereas in the southern hemisphere, they are positive during the WQBO and negative during the EQBO. The gravity wave-driven stream function anomalies are also opposite those under weak BSPV conditions (Figures 8b and 8e, Figures 6b and 6e). Similar to the weak BSPV conditions, the total stratospheric stream function anomalies are dominated by planetary wave-driven anomalies, whereas in the mesosphere, they are dominated by gravity wave-driven anomalies (Figures 8c and 8f).

Under strong BSPV conditions (Figure 9), the primary drivers of high-latitude w^* anomalies are consistent with the weak BSPV background. The anomalies in BDC intensity in the mesosphere are primarily driven by gravity wave anomalies, whereas in the stratosphere, they are mainly driven by planetary wave anomalies. However, the role of gravity waves in the upper stratosphere cannot be ignored, as their intensity is approximately half that of the planetary waves. Notably, gravity wave-driven anomalies oppose planetary wave-driven anomalies in the northern hemisphere, whereas they share the same polarity in the southern hemisphere. Under strong BSPV conditions, the BDC in the mesosphere is enhanced, with a more pronounced effect in the northern hemisphere during the WQBO and in the southern hemisphere during the EQBO (Figures 9a and 9j). In the northern hemisphere stratosphere, the BDC weakens, with a more significant effect in the upper stratosphere during the WQBO and in the lower stratosphere during the EQBO (Figures 9b and 9f). In the southern hemisphere stratosphere, the BDC is significantly modulated by the QBO under strong BSPV conditions: it weakens during the WQBO (Figures 9h and 9i) and strengthens during the EQBO (Figures 9k and 9l).

4. Summary and Discussion

Using the long-term simulation of the WACCM5 model containing complete stratospheric processes, we analyzed the anomalies of the BDC and the respective contributions of planetary and gravity waves under different combinations of the BSPV oscillation and the QBO at 10 hPa in NDJF, leading to the following conclusions, which are generalized in Figure 10. In NDJF, the stratosphere and mesosphere are jointly driven by planetary waves and gravity waves, which are very close to the actual BDC in the high latitudes of the northern and southern hemispheres (50°–80°). That is, the BDC here can be represented by the sum of the circulation driven by planetary waves and gravity waves.

The BDC in the northern hemisphere stratosphere exhibits stronger correlations with the BSPV, with the BDC strengthening (weakening) during a weak (strong) BSPV. The QBO can regulate the vertical position of the anomaly center of the BDC's descending branch. During the WQBO, the anomaly center of the descending branch is biased toward the upper stratosphere, whereas during the EQBO, it is biased toward the lower stratosphere.

The BDC in the southern hemisphere stratosphere is linked to both the QBO and BSPV. When the WQBO is combined with a weak (strong) BSPV, the southern hemisphere stratosphere exhibits an enhancement (weakening) of the poleward circulation, which is similar to that in the northern hemisphere stratosphere but with a slight anomaly intensity. Conversely, when the

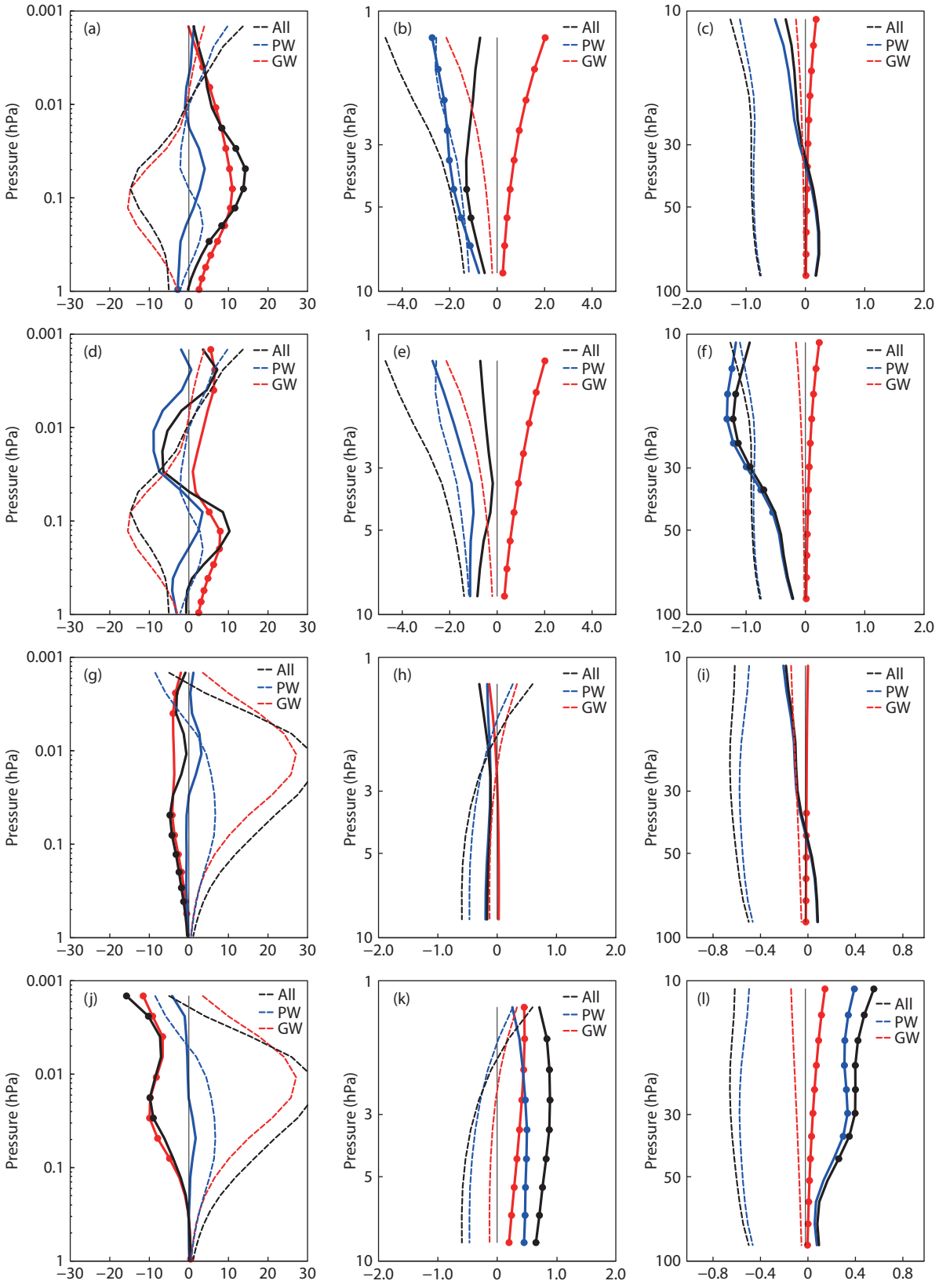

Figure 7. Climatology of the vertical residual velocity w^*, which is the meridional gradient of the mass stream function ψ^* in NDJF (dashed curves; unit: 10^{-3} m·s^{-1}) and its anomaly in the context of a weak polar vortex (solid curves; unit: 10^{-3} m·s^{-1}). The blue lines show the part driven by planetary waves (PW), the red lines show the part driven by gravity waves (GW), and the black lines show the part driven by both (All), with the dotted portion of the region passing the 90% significance test. (a–c) During the WQBO at 70°N; (d–f) during the EQBO at 70°N; (g–i) during the WQBO at 70°S; (j–l) during the EQBO at 70°S.

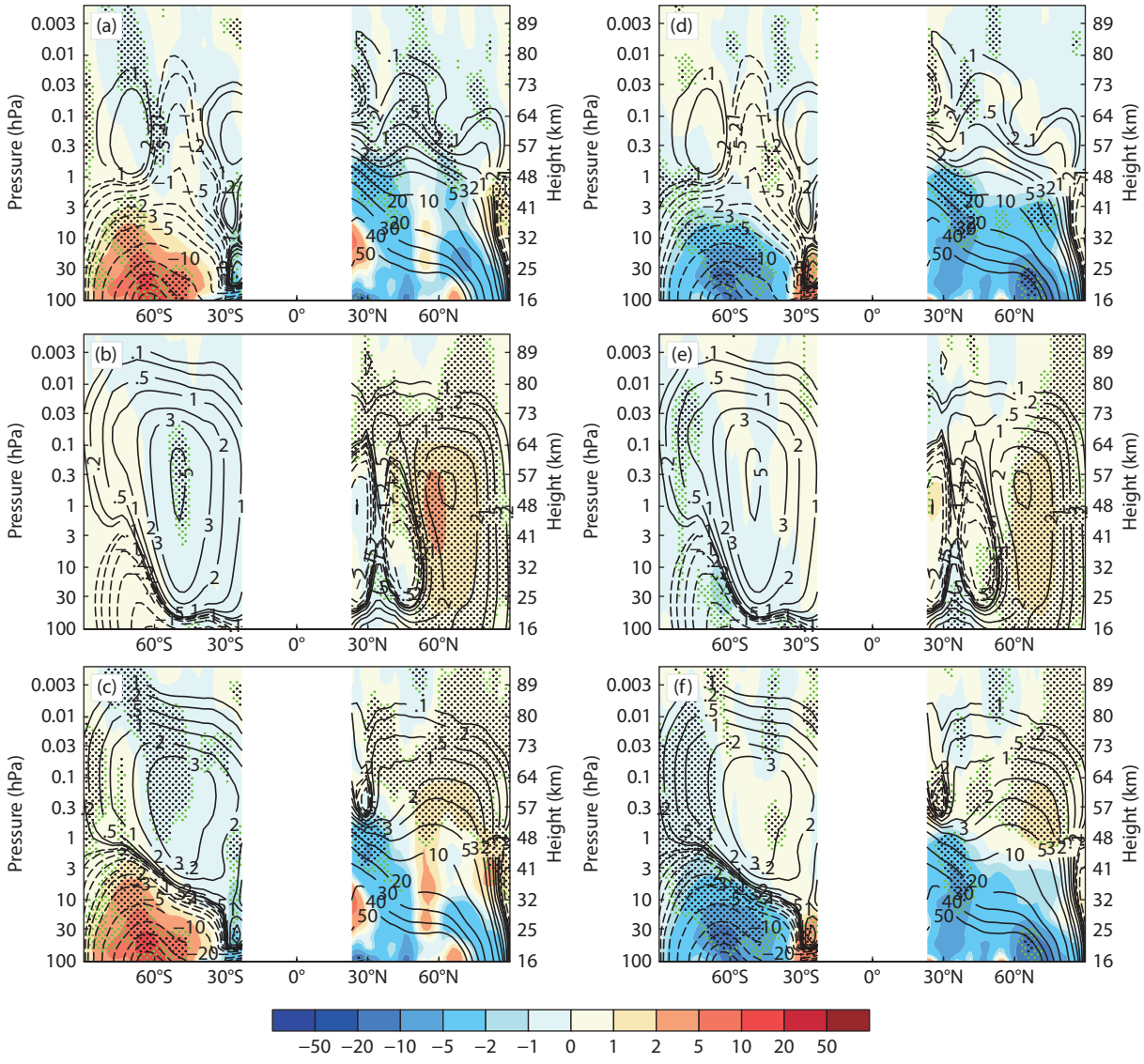

Figure 8. Climatology of the mass stream function in NDJF (contours; unit: kg·m^{-1}s^{-1}) and its anomaly (shaded; unit: kg·m^{-1}s^{-1}) under the background of a strong BSPV. (a) Mass stream function anomaly driven by planetary waves during the WQBO; (b) mass stream function anomaly driven by gravity waves during the WQBO; (c) mass stream function anomaly driven by both planetary and gravity waves during the WQBO; (d–f) as in (a) to (c), respectively, but during the EQBO.

EQBO is combined with a weak (strong) BSPV, the poleward circulation in the southern hemisphere stratosphere shows a weakening (enhancement), which is opposite that in the northern hemisphere stratosphere.

The mesosphere BDC weakens (strengthens) during a weak (strong) BSPV, and the anomaly is more significant in the northern hemisphere BDC during the WQBO and in the southern hemisphere BDC during the EQBO. The aforementioned BDC anomalies are primarily driven by gravity wave anomalies in the mesosphere, whereas in the stratosphere, the anomalies are primarily driven by planetary waves. However, the role of gravity waves in the upper stratosphere reaches approximately half that of the planetary wave effects. Furthermore, gravity wave-driven anomalies oppose planetary wave-driven anomalies in the northern hemisphere, whereas they share the same polarity in the southern hemisphere.

Acknowledgments

We acknowledge the High Performance Computing Center of Nanjing University of Information Science & Technology for their support of this work. This work was supported by the National Natural Science Foundation of China (Grant Nos. U2442210 42475072 and 42361144843).

References

Andrews, D. G., and McIntyre, M. E. (1976). Planetary waves in horizontal and vertical shear: The generalized Eliassen-Palm relation and the mean zonal acceleration. *J. Atmos. Sci.*, *33*(11), 2031–2048. https://doi.org/10.1175/1520-0469(1976)033<2031:pwihav>2.0.co;2

Anstey, J. A., and Shepherd, T. G. (2014). High-latitude influence of the quasi-biennial oscillation. *Quart. J. Roy. Meteor. Soc.*, *140*(678), 1–21. https://doi.org/10.1002/qj.2132

Azeem, S. M. I., Talaat, E. R., Sivjee, G. G., Liu, H. L., and Roble, R. G. (2005). Observational study of the 4-day wave in the mesosphere preceding the sudden stratospheric warming events during 1995 and 2002. *Geophys. Res.*

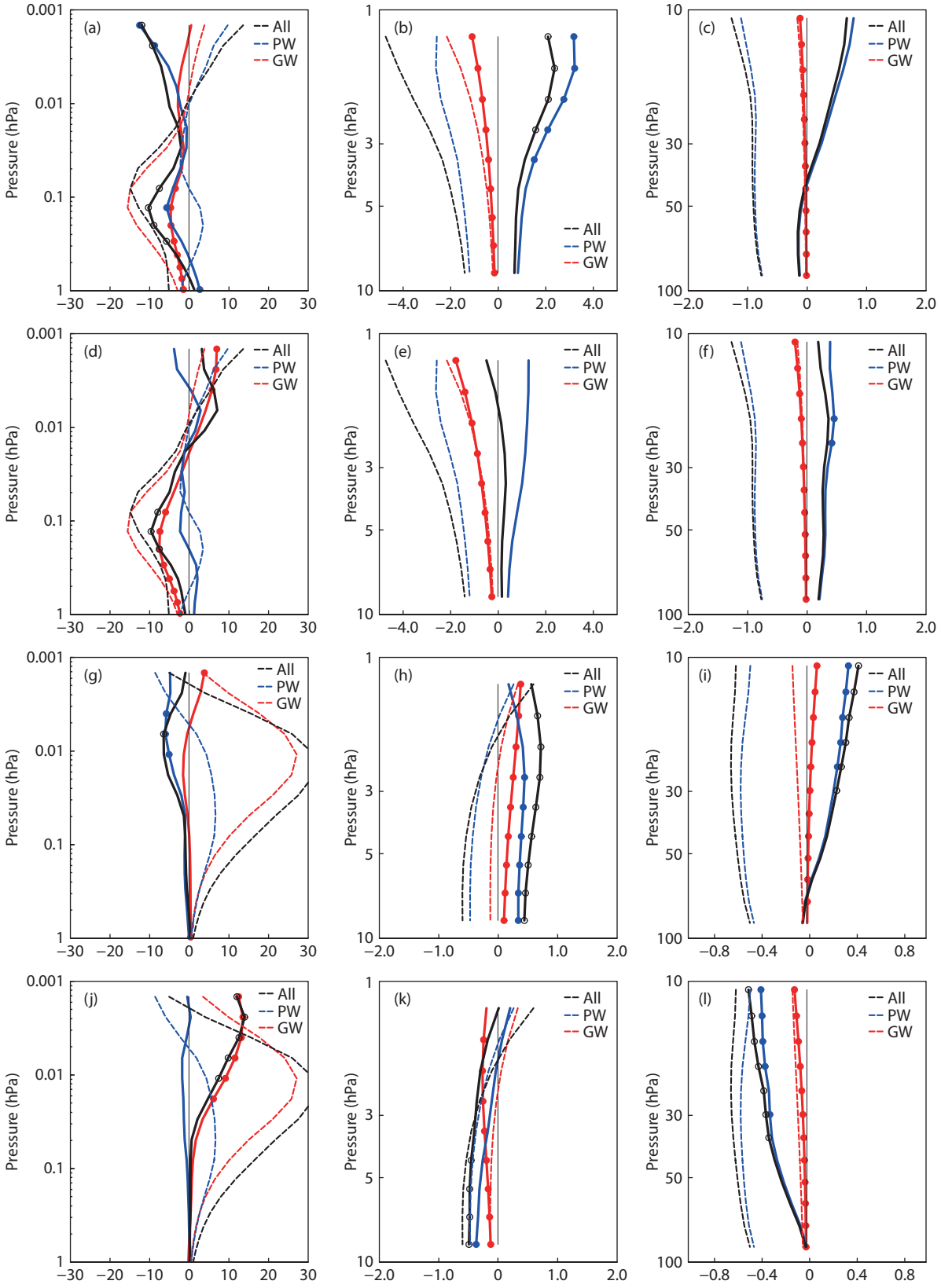

Figure 9. As in Figure 7, climatology of the vertical residual velocity w^* in NDJF (dashed curves; unit: 10^{-3} m·s^{-1}) and its anomaly in the context of a strong polar vortex (solid curves; unit: 10^{-3} m·s^{-1}). (a–c) During the WQBO at 70°N; (d–f) during the EQBO at 70°N; (g–i) during the WQBO at 70°S; (j–l) during the EQBO at 70°S.

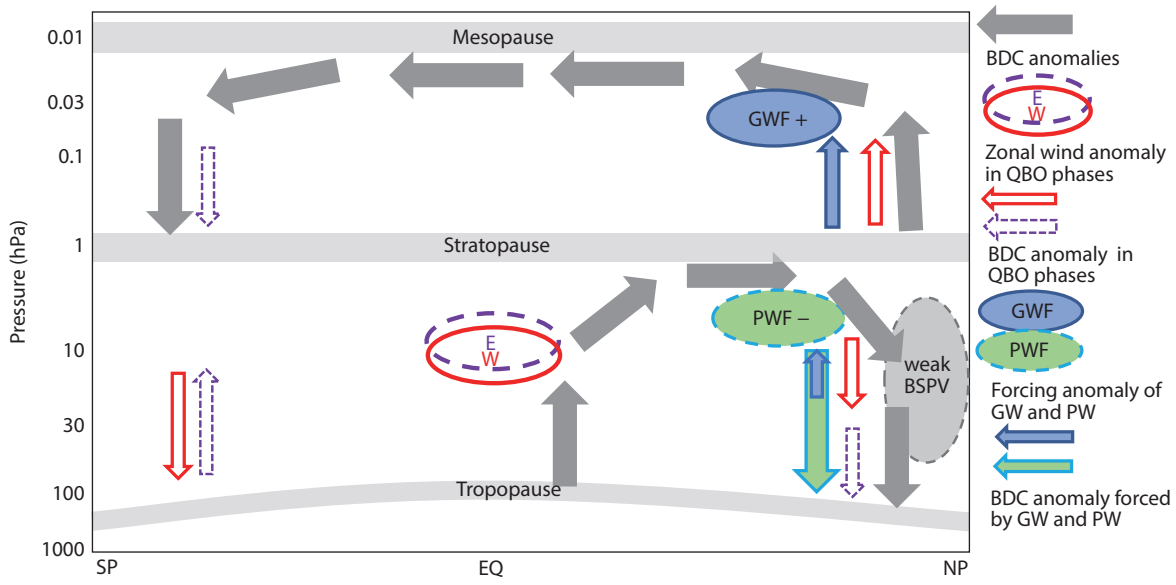

Figure 10. Conceptual diagram of the BDC anomaly forced by planetary waves (PW) and gravity waves (GW), and the BDC anomaly in EQBO and WQBO phases during a weak BSPV. The arrow direction and the forcing anomaly are opposite during a strong BSPV. GWF, gravity wave forcing; PWF, planetary wave forcing; SP, South Pole; EQ, equator; NP, North Pole.

Lett., *32*(15), L15804. https://doi.org/10.1029/2005gl023393

Baldwin, M. P., and Dunkerton, T. J. (2001). Stratospheric harbingers of anomalous weather regimes. *Science*, *294*(5542), 581–584. https://doi.org/10.1126/science.1063315

Birner, T., and Bönisch, H. (2011). Residual circulation trajectories and transit times into the extratropical lowermost stratosphere. *Atmos. Chem. Phys.*, *11*(2), 817–827. https://doi.org/10.5194/acp-11-817-2011

Butchart, N., and Scaife, A. A. (2001). Removal of chlorofluorocarbons by increased mass exchange between the stratosphere and troposphere in a changing climate. *Nature*, *410*(6830), 799–802. https://doi.org/10.1038/35071047

Butchart, N., Scaife, A. A., Bourqui, M., de Grandpré, J., Hare, S. H. E., Kettleborough, J., Langematz, U., Manzini, E., Sassi, F., … Sigmond, M. (2006). Simulations of anthropogenic change in the strength of the Brewer–Dobson circulation. *Climate Dyn.*, *27*(7-8), 727–741. https://doi.org/10.1007/s00382-006-0162-4

Butchart, N., Cionni, I., Eyring, V., Shepherd, T. G., Waugh, D. W., Akiyoshi, H., Austin, J., Brühl, C., Chipperfield, M. P., … Tian, W. (2010). Chemistry–climate model simulations of twenty-first century stratospheric climate and circulation changes. *J. Climate*, *23*(20), 5349–5374. https://doi.org/10.1175/2010jcli3404.1

Butchart, N. (2014). The Brewer-Dobson circulation. *Rev. Geophys.*, *52*(2), 157–184. https://doi.org/10.1002/2013rg000448

Butchart, N. (2022). The stratosphere: A review of the dynamics and variability. *Wea. Climate Dyn.*, *3*(4), 1237–1272. https://doi.org/10.5194/wcd-3-1237-2022

Cai, Q. Y., Chen, W., Chen, S. F., Ma, T. J., and Garfinkel, C. I. (2022). Influence of the quasi-biennial oscillation on the spatial structure of the wintertime Arctic Oscillation. *J. Geophys. Res.: Atmos.*, *127*(8), e2021JD035564. https://doi.org/10.1029/2021jd035564

Chandran, A., Garcia, R. R., Collins, R. L., and Chang, L. C. (2013). Secondary planetary waves in the middle and upper atmosphere following the stratospheric sudden warming event of January 2012. *Geophys. Res. Lett.*, *40*(9), 1861–1867. https://doi.org/10.1002/grl.50373

de Wit, R. J., Hibbins, R. E., Espy, P. J., and Hennum, E. A. (2015). Coupling in the middle atmosphere related to the 2013 major sudden stratospheric warming. *Annales Geophysicae*, *33*(3), 309–319. https://doi.org/10.5194/angeo-33-309-2015

Diallo, M., Ern, M., and Ploeger, F. (2021). The advective Brewer–Dobson circulation in the ERA5 reanalysis: Climatology, variability, and trends. *Atmospheric Chemistry and Physics*, *21*(10), 7515–7544. https://doi.org/10.5194/acp-21-7515-2021

Garfinkel, C. I., Shaw, T. A., Hartmann, D. L., and Waugh, D. W. (2012). Does the Holton–Tan mechanism explain how the quasi-biennial oscillation modulates the arctic polar vortex?. *J. Atmos. Sci.*, *69*(5), 1713–1733. https://doi.org/10.1175/jas-d-11-0209.1

Haynes, P. H., McIntyre, M. E., Shepherd, T. G., Marks, C. J., and Shine, K. P. (1991). On the "downward control" of extratropical diabatic circulations by eddy-induced mean zonal forces. *J. Atmos. Sci.*, *48*(4), 651–678. https://doi.org/10.1175/1520-0469(1991)048<0651:otcoed>2.0.co;2

Holton, J. R., and Tan, H. C. (1980). The influence of the equatorial quasi-biennial oscillation on the global circulation at 50 mb. *J. Atmos. Sci.*, *37*(10), 2200–2208. https://doi.org/10.1175/1520-0469(1980)037<2200:tioteq>2.0.co;2

Holton, J. R., and Tan, H. C. (1982). The quasi-biennial oscillation in the Northern Hemisphere lower stratosphere. *J. Meteor. Soc. Japan*, *60*(1), 140–148. https://doi.org/10.2151/jmsj1965.60.1_140

Kolstad, E. W., Breiteig, T., and Scaife, A. A. (2010). The association between stratospheric weak polar vortex events and cold air outbreaks in the Northern Hemisphere. *Quart. J. Roy. Meteor. Soc.*, *136*(649), 886–893. https://doi.org/10.1002/qj.620

Limpasuvan, V., Thompson, D. W. J., and Hartmann, D. L. (2004). The life cycle of the northern hemisphere sudden stratospheric warmings. *Journal of Climate*, *17*(13), 2584–2596. https://doi.org/10.1175/1520-0442(2004)017<2584:tlcotn>2.0.co;2

Li, F., Austin, J., and Wilson, J. (2008). The strength of the Brewer–Dobson circulation in a changing climate: Coupled chemistry–climate model simulations. *J. Climate*, *21*(1), 40–57. https://doi.org/10.1175/2007jcli1663.1

Li, Q., Graf, H. F., and Cui, X. F. (2011). The role of stationary and transient planetary waves in the maintenance of stratospheric polar vortex regimes in Northern Hemisphere winter. *Adv. Atmos. Sci.*, *28*(1), 187–194. https://doi.org/10.1007/s00376-010-9163-7

Martineau, P., and Son, S. W. (2010). Quality of reanalysis data during stratospheric vortex weakening and intensification events. *Geophys. Res. Lett.*, *37*(22), L22801. https://doi.org/10.1029/2010GL045237

McLandress, C., and Shepherd, T. G. (2009). Simulated anthropogenic changes in the Brewer–Dobson circulation, including its extension to high latitudes. *J. Climate*, *22*(6), 1516–1540. https://doi.org/10.1175/2008jcli2679.1

Rao, J., Yu, Y. Y., Guo, D., Shi, C. H., Chen, D., and Hu, D. Z. (2019). Evaluating the Brewer–Dobson circulation and its responses to ENSO, QBO, and the solar

cycle in different reanalyses. *Earth Planet. Phys.*, *3*(2), 166–181. https://doi.org/10.26464/epp2019012

Rao, J., and Garfinkel, C. I. (2020). Arctic ozone loss in March 2020 and its seasonal prediction in CFSv2: A comparative study with the 1997 and 2011 cases. *J. Geophys. Res.: Atmos.*, *125*(21), e2020JD033524. https://doi.org/10.1029/2020JD033524

Rosenlof, K. H., and Holton, J. R. (1993). Estimates of the stratospheric residual circulation using the downward control principle. *J. Geophys. Res.: Atmos.*, *98*(D6), 10465–10479. https://doi.org/10.1029/93jd00392

Sato, K., and Hirano, S. (2019). The climatology of the Brewer–Dobson circulation and the contribution of gravity waves. *Atmos. Chem. Phys.*, *19*(7), 4517–4539. https://doi.org/10.5194/acp-19-4517-2019

Tian, W. S., Huang, J. L., Zhang, J. K., Xie, F., Wang, W. K., and Peng, Y. F. (2023). Role of stratospheric processes in climate change: Advances and challenges. *Adv. Atmos. Sci.*, *40*(8), 1379–1400. https://doi.org/10.1007/s00376-023-2341-1

Tomikawa, Y., Sato, K., Watanabe, S., Kawatani, Y., Miyazaki, K., and Takahashi, M. (2012). Growth of planetary waves and the formation of an elevated stratopause after a major stratospheric sudden warming in a T213L256 GCM. *J. Geophys. Res.: Atmos.*, *117*(D16), D16101. https://doi.org/10.1029/2011jd017243

Xie, F., Zhang, J. K., Li, X. T., Li, J., Wang, T., and Xu, M. (2020). Independent and joint influences of eastern Pacific El Niño–southern oscillation and quasi-biennial oscillation on Northern Hemispheric stratospheric ozone. *Int. J. Climatol.*, *40*(12), 5289–5307. https://doi.org/10.1002/joc.6519

Xie, F., Ma, X., Li, Y. J., Li, J. P., Chen, X. S., Tian, W. S., Sun, C., Xu, M., Zhang, J. K., … Niu, Y. L. (2024). Southern hemispheric jet swing linked to arctic stratospheric polar vortex. *Environ. Res. Lett.*, *19*(4), 044053. https://doi.org/10.1088/1748-9326/ad3460

Yu, F. R., Huang, K. M., Zhang, S. D., Huang, C. M., Yi, F., Gong, Y., Wang, R., Li, G. Z., and Ning, B. Q. (2019). Quasi 10- and 16-day wave activities observed through meteor radar and MST radar during stratospheric final warming in 2015 spring. *J. Geophys. Res.: Atmos.*, *124*(12), 6040–6056. https://doi.org/10.1029/2019jd030630

Zhang, C. Y., Zhang, J. K., Xia, X. F., Song, J. B., Li, D. W., and Tian, W. S. (2024). Impacts of stratospheric polar vortex changes on tropospheric blockings over the Atlantic region. *Climate Dyn.*, *62*(6), 4829–4848. https://doi.org/10.1007/s00382-023-07092-z

Zhang, J. K., Zhang, C. Y., Zhao, S. Y., Liu, Y. X., Du, S. H., Wang, W. K., Huang, J. L., and Xu, M. (2023). Impacts of the Arctic stratospheric polar vortex changes on the frontogenesis over the northern middle latitudes during winter. *Atmos. Res.*, *289*, 106751. https://doi.org/10.1016/j.atmosres.2023.106751

Zhang, R. H., Tian, W. S., and Wang, T. (2020). Role of the quasi-biennial oscillation in the downward extension of stratospheric northern annular mode anomalies. *Climate Dyn.*, *55*(3-4), 595–612. https://doi.org/10.1007/s00382-020-05285-4